Experimental and numerical characterization of timing jitter for short electron beams in a linear photo-injector

Experimental and numerical characterization of timing jitter for short electron beams in a linear photo-injector

G. Giannetti[1], M. P. Anania[2], M. Bellaveglia[2], E. Chiadroni[6,7], A. Cianchi[3,4], A. Del Dotto[2], M. Galletti[3,4,5], A. Gallo[2], A. Giribono[2], L. Piersanti[2], R. Pompili[2], S. Romeo[2], B. Serenellini[2], S. Tocci[2], C. Vaccarezza[2], F. Villa[2] and M. Ferrario[2]

[1]Department of Information Engineering, University of Florence, Piazza San Marco 4, I-50121 Florence, Italy
[2]Laboratori Nazionali di Frascati, Via Enrico Fermi 54, I-00044 Frascati (Rome), Italy
[3]Department of Physics, Tor Vergata University, Via Ricerca Scientifica 1, I-00133 Rome, Italy
[4]INFN Tor Vergata, Via Ricerca Scientifica 1, I-00133 Rome, Italy
[5]NAST Center, Via Ricerca Scientifica 1, I-00133 Rome, Italy
[6]Dipartimento SBAI, Università di Roma La Sapienza, Via A. Scarpa 14, 00161 Roma, Italy
[7]INFN Sezione di Roma, 00185 Roma, Italy

E-mail: giacomo.giannetti@unifi.it

Abstract. In modern particle accelerators involving short (few hundreds of fs or less) photon and particle beams, a crucial requirement is the arrival timing jitter and its modeling, taking into account different noise sources. This paper considers the arrival timing jitter of an electron beam measured at the SPARC_LAB photo-injector test facility (INFN-LNF, Frascati) and studies how the different jitter sources impact on the beam arrival time, considering three velocity bunching machine working points. This study includes the development of a first order mathematical model that describes the jitter contributions, the PIC code simulations for the machine working point description and experimental data acquired in a dedicated run at SPARC_LAB to benchmark both the proposed model and simulations.

Keywords: beam dynamics, synchronization, timing jitter, velocity-bunching

Submitted to: *Meas. Sci. Technol.*

1. Introduction and motivation

Recent experiments involving particle beams interacting with high power laser pulses push the synchronization system requirements to the limit. In particular, when very

short (few hundreds of fs or less) particle and laser beams have to interact, the beam arrival timing jitter (BATJ) between these pulses should be of the order of few tens femtoseconds or better. For instance, this is the case in plasma wakefield acceleration (PWFA) [1] and in pump and probe free electron laser (FEL) experiments characterized by a small-time resolution [2]. To match such a stringent specification, it is important to understand how the timing jitter of the different accelerator sub-systems can affect the beam arrival time (BAT) at a specified location (e.g., interaction point).

In [3], a mathematical model of the jitter propagation is reported together with experimental measurements of BATJ for hybrid compression configuration (RF and magnetic) of the photo-injector at the SPARC_LAB test-facility (INFN-LNF, Frascati). In [4], the BATJ is studied from both an analytical and a measurement point of view considering magnetic compression. In [5], the BATJ in sub-relativistic pump-probe ultrafast electron diffraction (UED) is studied only from a theoretical point of view. In [6], THz beam compression is analyzed to reduce femtosecond relativistic electron beams for UED and FEL experiments. In [7], RF cavities are employed to reduce the limit of temporal resolution in UED accelerators.

In this paper we report about the use of a simple BATJ linear model at SPARC_LAB photo-injector for three different machine working points (WPs) (i.e., three different RF compression regimes), together with the respective simulations made with the TStep code [8] and the experimental data. These WPs are of special interest for the research being conducted at SPARC_LAB. An impact analysis of the various sub-system jitters on the overall BATJ is also reported. The novelties of the work are that it provides more accurate measurements of BATJ coefficients and that it characterizes both numerically and experimentally the BATJ coefficients of slightly different WPs. Additionally, it supplies specific calibration data for the SPARC_LAB test-facility and reference data for other facilities exploiting RF compression.

The paper is organized as follows. In section 2 the test facility is described and features relevant to the scope of this work are introduced. Then in section 3 BATJ is theoretically modelled and in section 4 the setups of both experiments and simulations are supplied. Eventually, results and discussion are exposed in section 5 while conclusions are drawn in section 6.

2. SPARC_LAB test-facility

SPARC_LAB [9] at LNF-INFN is a test-facility supplying electron bunches with energy up to 170 MeV feeding several experimental beamlines. In this facility plasma acceleration schemes and leading-edge research activities based on novel radiation sources, e.g., [10, 11], are investigated. The electron source consists of an S-band (2856 MHz) 1.6 cell BNL/UCLA/SLAC type RF-gun supplying 120 MV/m peak electric field on the built-in copper photo-cathode (PC). Electrons are extracted by means of UV laser pulses (wavelength: 266 nm, photon energy: 4.66 eV) whose shape and duration can be tailored to the needs of the aforementioned applications. Particles are accelerated

up to 5.3 MeV in the gun [12] and then injected into two S-band sections (called S1, and S2 in the following). S1 is also used as RF-compressor by means of the velocity bunching (VB) technique [13, 14]. Solenoid coils embedding the first two S-band sections provide additional magnetic focusing and control of the emittance and envelope oscillations, particularly useful in case of VB operation [15]. A C-band (5712 MHz) accelerating section is then used as booster, to achieve the nominal kinetic energy. The gun is fed by klystron 1 (K1), sections S1 and S2 by klystron 2 (K2) and section C by klystron 3 (K3).

At SPARC_LAB, the BATJ can be measured by two instruments: a radio frequency deflecting cavity (RFD) [16], and an electro-optical sampling (EOS) system [17]. The former is fed by K1 and measures the jitter relative to the phase of K1; the latter measures the jitter relative to the PC laser since the EOS laser is derived from the amplification chain of the PC laser. The scheme of the linear accelerator is shown in figure 1.

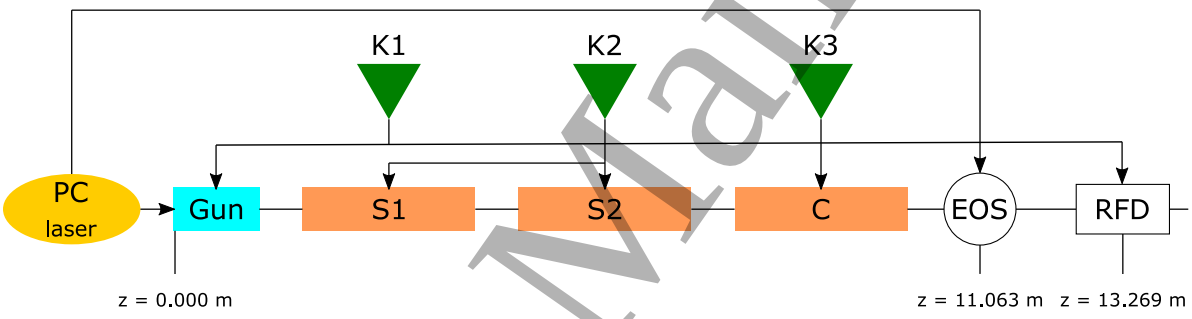

Figure 1: Scheme of the linear accelerator. The arrows indicate the directions of the feeding lines for the different subsystems.

3. Theoretical background

The BAT is influenced by RF field fluctuations in the accelerating structures, resulting in a BATJ at the end of the line. Another source of jitter, in case of photo-injectors, is linked to the arrival time of the PC laser. The BATJ is defined as the shot-to-shot time of arrival fluctuation of the beam center of mass with respect to a fixed longitudinal position along the machine. At SPARC_LAB the BATJ is mainly produced by four sources, listed in table 1.

The BAT $t_{\text{linac}}(t_1, t_2, t_3, t_4)$ is a function of the times t_i at which the different sources are activated. The index $i = 1, 2, 3, 4$ refers, respectively, to the PC laser, K1, K2, and K3. Once that a WP is fixed, the start times for the different sources are also fixed and the Taylor expansion for the BAT is:

$$t_{\text{linac}}(\mathbf{t}) = t_{\text{linac}}(\bar{\mathbf{t}}) + \nabla t_{\text{linac}} \cdot \Delta\mathbf{t} + o(||\Delta\mathbf{t}||) \tag{1}$$

where $\mathbf{t} = (t_1, t_2, t_3, t_4)$, $\bar{\mathbf{t}} = (\bar{t}_1, \bar{t}_2, \bar{t}_3, \bar{t}_4)$, $\Delta\mathbf{t} = (\Delta t_1, \Delta t_2, \Delta t_3, \Delta t_4)$ and ∇t_{linac} is the gradient of t_{linac} evaluated in $\bar{\mathbf{t}}$. For the sake of clarity, we call c_i the derivative of t_{linac} with respect to the ith component evaluated in $\mathbf{t} = \bar{\mathbf{t}}$. Then it is: $\nabla t_{\text{linac}} = (c_1, c_2, c_3, c_4)$.

Table 1: Sub-system jitter sources and elements on which they impact.

Source	Impacts on	Symbol	Measured jitter [fs] (rms)
Laser	Photocathode, EOS	σ_{t_L}	≈ 35
S-band klystron 1 (K1)	Gun cavity, RFD	$\sigma_{t_{K1}}$	≈ 45
S-band klystron 2 (K2)	S-band section 1, and 2	$\sigma_{t_{K2}}$	≈ 85
C-band klystron (K3)	C-band section	$\sigma_{t_{K3}}$	≈ 30

The coefficients c_i are defined as the partial derivative of t_{linac} at a certain time, hence they depend on the specific WP.

Neglecting higher order terms, writing $\Delta t_{\text{linac}}(\mathbf{t}, \bar{\mathbf{t}}) = t_{\text{linac}}(\mathbf{t}) - t_{\text{linac}}(\bar{\mathbf{t}})$ and expanding the dot product we get

$$\Delta t_{\text{linac}} \approx \sum_{i=1}^{4} c_i \Delta t_i. \tag{2}$$

If the laser and the RF fields are delayed all together by a given value Δt, the relative differences between laser and RF fields do not change and it follows that [3]: a) the BAT is delayed by the same amount, and b) the final energy of the beam remains unchanged. Point a) can be expressed mathematically as $\Delta t_{\text{linac}}(\mathbf{t}, \bar{\mathbf{t}}) = \Delta t_{\text{linac}}(\mathbf{t} + \Delta\hat{\mathbf{t}}, \bar{\mathbf{t}} + \Delta\hat{\mathbf{t}})$ where $\Delta\hat{\mathbf{t}} = (\Delta t, \Delta t, \Delta t, \Delta t)$. Applying condition a) to (2) the following constraint on coefficients c_i is found

$$\sum_{i=1}^{4} c_i \approx 1. \tag{3}$$

However, if there are strong non-linear terms, (3) is not fulfilled in general.

All Δt_i values are measured with respect to the reference master oscillator (RMO). Since they are mostly uncorrelated [3], from (2) the expected BATJ (with respect to the RMO) at the linac exit writes

$$\sigma^2_{t_{\text{linac}}} \approx \sum_{i=1}^{4} c_i^2 \sigma^2_{t_i}. \tag{4}$$

In general, a BATJ measuring device can provide a BATJ measurement only relative to a subsystem reference. If $\Delta t'$ is the time difference measured by an instrument and Δt_j the delta time of the subsystem feeding that instrument, then we have:

$$\Delta t' = \Delta t_{\text{linac}} - \Delta t_j. \tag{5}$$

Indeed, if the measuring instrument is delayed, it measures a shorter time interval. To estimate a single coefficient c_i at a time, only a single source is delayed or anticipated; that is:

$$\Delta t' = c_i \Delta t_i - \Delta t_j. \tag{6}$$

If the source feeding the measuring instrument is different from the source that is delayed or anticipated, then Δt_j vanishes, since only a source is delayed or anticipated at a time. Otherwise, if the source of the measuring system coincides with the one that is delayed or anticipated, then $\Delta t_j = \Delta t_i$ and (6) becomes

$$\Delta t' = c_i \Delta t_i - \Delta t_i = (c_i - 1)\Delta t_i. \tag{7}$$

The sought coefficient c_i is then equal to one plus the angular coefficient of the line fitting the points Δt_i for the x-axis and the points $\Delta t'$ for the y-axis.

The total absolute jitter of the beam can be expressed as a linear combination of several jitter sources, as indicated by (2). However, (2) needs to be changed depending upon the instrument used for the measurements. Indeed, if the BATJ downstream the linac is measured with the RFD, this will be relative to the RF line 1 and (4) becomes

$$\sigma_{t_{\mathrm{RFD}}} \approx \sqrt{c_1^2\sigma_{t_L}^2 + (c_2 - 1)^2\sigma_{t_{K1}}^2 + c_3^2\sigma_{t_{K2}}^2 + c_4^2\sigma_{t_{K3}}^2} \tag{8}$$

with $\sigma_{t_L}^2 = \sigma_{t_1}^2$ the jitter of the laser, and $\sigma_{t_{Ki}}^2 = \sigma_{t_{i+1}}^2$, $i = 1, 2, 3$ the jitter of the ith RF line. On the other hand, measuring the BATJ with the EOS will return the jitter relative to the PC laser and (4) becomes

$$\sigma_{t_{\mathrm{EOS}}} \approx \sqrt{(c_1 - 1)^2\sigma_{t_L}^2 + c_2^2\sigma_{t_{K1}}^2 + c_3^2\sigma_{t_{K2}}^2 + c_4^2\sigma_{t_{K3}}^2}. \tag{9}$$

4. Setups of experiments and simulations

4.1. Setup of the photo-injector and beam parameters for the WPs

In this paper, three WPs are considered: VB operation very close to the maximum RF compression phase (i.e., minimum bunch length at the exit of the first accelerating section) [13, 14] and RF compression regimes choosing a phase three and six degrees toward the crest, i.e., the maximum energy gain regime, respect to VB (named VB3 and VB6, respectively). The transverse and longitudinal properties of the PC laser pulse and the charge of the electron beam are kept constant in all WPs and are listed in table 2. The beam parameters for the three different WPs are listed in table 3. For the normalized transverse emittance measured values are available only for VB6.

In figure 2 the simulated longitudinal phase space (LPS) for the three considered WPs is reported. In particular, the ratio $(E - \langle E\rangle)/\langle E\rangle = \Delta E/\langle E\rangle$ with E the particle energy and $\langle E\rangle$ the mean beam energy is plotted against the difference between particle arrival times, t, and the mean BAT, $\langle t\rangle$, at the end of the linac. As expected, the VB is the one characterized by the shortest duration, while this increases going towards the crest. An analogous trend is observed for the energy spread too.

4.2. Experimental runs and instruments

To obtain the values of the c_i coefficients from measurements, the phases relative to the RMO of (i) the PC laser, (ii) the klystron 1 RF line (feeding the RF gun and the

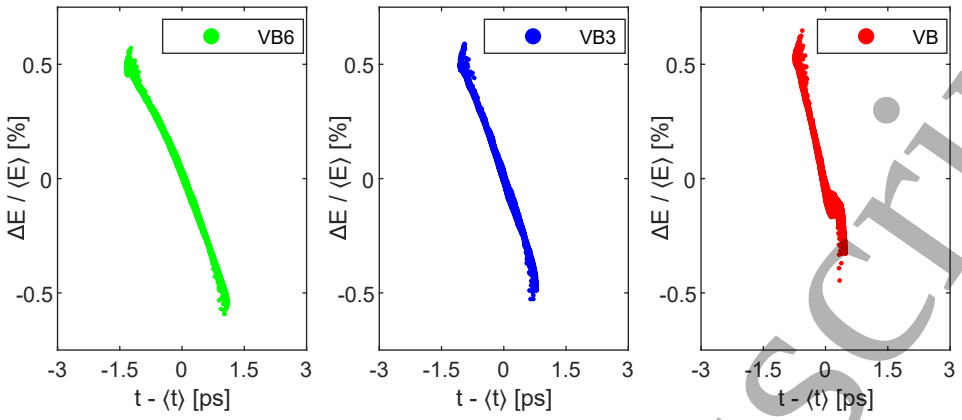

Figure 2: Simulated LPS at the end of the linac for the three WPs.

Table 2: Measured (Meas.) and simulated (Sim.) laser and beam parameters.

Laser parameters	Meas.	Sim.	Unit
X spot (rms)	248.5	248.5	µm
Y spot (rms)	335.5	335.5	µm
Pulse duration (rms)	130	130	fs
Beam parameters	**Meas.**	**Sim.**	**Unit**
Charge	150	150	pC

Table 3: Measured (Meas.) and simulated (Sim.) beam parameters (Beam par.) at the end of the linac: mean energy, $\langle E \rangle$; energy spread, σ_E; duration, σ_t; normalized transverse emittance, ε.

Beam par.	WP VB		WP VB3		WP VB6		Unit
	Meas.	Sim.	Meas.	Sim.	Meas.	Sim.	
$\langle E \rangle$	85.95	85.76	88.33	88.23	90.44	90.45	MeV
σ_E (rms)	130	130	200	192	240	218	keV
σ_t (rms)	277	273	413	418	569	554	fs
ε (rms)	n/a	1.4	n/a	1.7	1.7	1.7	mm·mrad

deflector) and (iii) the klystron 2 RF line (feeding the first two accelerating sections), are shifted, one at a time, by fixed steps of 0.5 deg in a range of ±1 deg (at 2856 MHz a 1-deg shift corresponds to a time shift of $1000/(360 \cdot 2.856)$ ps ≈ 0.9726 ps) and the relative BAT is recorded. The BATJ coefficients are then given by the slope of the line fitting the relative BAT versus the time shifts of the different sub-systems.

The measurements of BATJ are performed by the RFD and the EOS. To obtain the relative BAT from raw measurements data processing is needed. In particular, since the RFD kicks the beam in the vertical axis, and the intensity of the kick changes according to the phase of the cavity fields, a different BAT reflects in a different deflecting force experienced by the particles. Measuring the position of the vertical centroid of the beam on a fluorescent screen placed downstream the RFD after a drift space, we can derive the BATJ relative to the RF line feeding the RFD. The calibration coefficients, $\mathrm{Cal_{fit}}$, and the errors on the calibration coefficients, $\mathrm{Cal_{err}}$, are listed in table A1. For further details and instances of raw data processing reader is referred to [16, 18].

In the EOS the electron beam electric field interacts with a laser pulse spilled from the PC laser amplification chain, by means of a birefringent crystal placed inside the vacuum chamber alongside the beam trajectory. In this case the images of the beam are acquired on a calibrated screen too. According to BAT at the crystal, respect to the laser, the images are shifted on a defined axis, that is a projection of the longitudinal axis of the beam trajectory. Additionally, an optical delay line is used to guarantee the superposition in time of particle beam and laser pulse at the crystal. Then the relative BAT is given by:

$$\mathrm{EOS_{meas}} = \mathrm{EOS_{read}} + \frac{2 \cdot \mathrm{EOS_{dl}}}{c} \tag{10}$$

with $\mathrm{EOS_{meas}}$ the relative measured BAT, $\mathrm{EOS_{read}}$ the reading of the instrument, $\mathrm{EOS_{dl}}$ the length of the delay line and c the speed of light in vacuum. For examples of raw data and their elaboration to get $\mathrm{EOS_{read}}$ reader is referred to [17, 19, 20].

Regarding the uncertainties of the measurements, the absolute error for RFD measurements is:

$$\mathrm{RFD_{err}[ps]} = \left| \mathrm{RFD_{read}[mm]} \cdot \mathrm{Cal_{fit}[ps/mm]} \left(\frac{\mathrm{RFD_{err}[mm]}}{\mathrm{RFD_{read}[mm]}} + \frac{\mathrm{Cal_{err}[ps/mm]}}{\mathrm{Cal_{fit}[ps/mm]}} \right) \right| \tag{11}$$

with $\mathrm{RFD_{read}}$ ($\mathrm{RFD_{err}}$) the reading (error in the reading) of the RFD. On the other hand, the absolute error for the EOS measurements, $\mathrm{EOS_{err}}$, is equal to the absolute error of $\mathrm{EOS_{read}}$ in (10), since the length of the delay line is considered not affected by errors.

The phases set to perform the measurements are affected by uncertainties too. These are represented by the rms phase jitter measured with respect to the facility master reference and reported in table 1. The klystron jitters are measured by means of the low level RF (LLRF) system. Each LLRF module receives the signal from a directional coupler placed in the waveguide network downstream the corresponding klystron. In particular, an average phase is calculated for each RF pulse and the standard deviation of about 100 consecutive shots (≈ 10 seconds) is reported. The

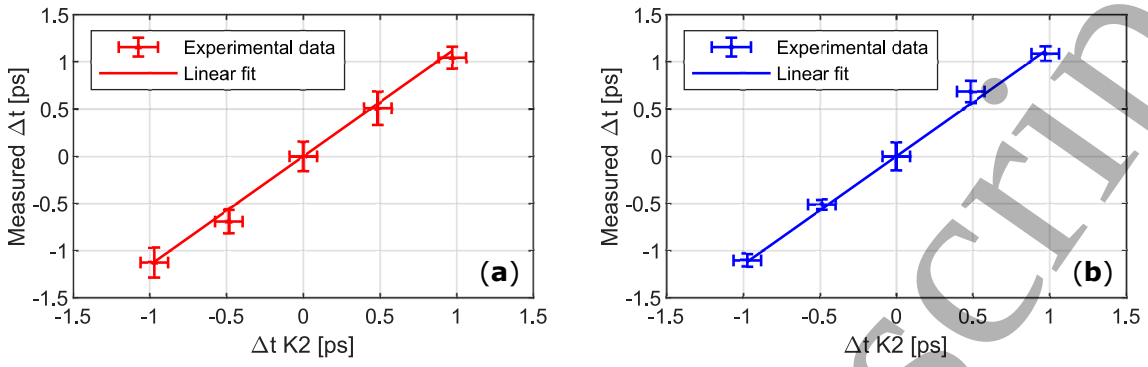

Figure 3: Experimental data and linear fit from measurements for c_3 coefficient for VB WP: (**a**), RFD; (**b**), EOS. Horizontal and vertical bars represent the time uncertainty due to jitter and measurement uncertainty, respectively.

timing jitter of the PC laser is measured at the infrared oscillator output. An electric comb signal is generated by a fast photo-detector and it is band-pass filtered to extract a CW signal at the S-band RF frequency. Then, again, a receiver channel of a S-band LLRF module is used to measure the phase noise. In our discussion we do not consider fluctuations in the amplitude of RF fields, since their contribution for short electron bunches is negligible when compared to phase jitter, as indicated in [3] and confirmed by simulations for the present case‡.

4.3. Data analysis

The experimental data elaborated according to section 4.2 are listed in Appendix A (tables from A2 to A7). For each WP, a set of 5 BATJ measurements corresponding to the 5 different time delays applied on purpose to a subsystem is performed. Data are then linear-fitted neglecting second order effects and considering the delay applied to the subsystem (measured timing jitter) as independent (dependent) variable. The angular coefficient of the fitting line is an experimental estimation of the BATJ coefficient c_i introduced in section 3, relative to the subsystem to which the time delay is applied. The measured values and uncertainties on the evaluation of the BATJ coefficients are evaluated by means of the Monte Carlo method (measured quantities are assumed to have a Gaussian distribution with mean equal to the measured value and variation equal to the absolute error).

In figure 3 the measurements and the linear interpolation used to calculate the c_3 coefficient (relative to RF line 2) are reported as example. The horizontal error bars represent the uncertainty on the applied time delay while the vertical error bars represent the absolute error from measurement.

‡ The RF amplitude jitter is $\Delta V_{\mathrm{RF}}/V_{\mathrm{RF}} \approx 0.08\,\%$. The simulated coefficients for the VB WP due to amplitude jitter with respect to the PC laser and klystrons K1 and K2 are $-99\,\mathrm{fs}/\%$ and $-122\,\mathrm{fs}/\%$, respectively. The expected amplitude timing jitters are then less than 8 fs and 10 fs, respectively.

4.4. Simulations

The measured WPs are reproduced by means of beam dynamics simulations with TStep code [8]. TStep is a multi-particle tracking code that takes into account space charge effects, relevant at very low energies, the beam loading and the beam features defined in the emission from the PC. In simulations $3 \cdot 10^4$ macro-particles are considered, being a good compromise between accuracy and computation time.

The results of the simulations are reported in brackets in table 3 and show an excellent agreement with the experimental data. After the WPs validation, simulations are also performed to reproduce the BATJ values and c_i coefficients. As in measurements, the PC laser time of arrival and the RF accelerating phases are delayed or anticipated one at a time, and the times at which particles cross a virtual screen located at the exit of the linac (12 m far away from the cathode) are recorded. The BAT is then calculated as the average of the times of the particles crossing the screen.

5. Results and discussion

5.1. BATJ coefficients

The BATJ coefficients, obtained by measurements and simulations, are listed in table 4 for VB WP and in table 5 for VB3 and VB6 WPs. K3 has a negligible impact on the BAT since it feeds the last C-band section that is used only on crest as energy booster. This fact is confirmed by simulations since the simulated c_4 coefficients are zero for all WPs. For this reason, c_4 coefficient measurements have not been performed.

In general, we observe a very good agreement between simulations and experimental data. Indeed, simulations and measurements from both EOS and RFD are always compatible within measurements errors for all WPs. Regarding uncertainties, EOS measurements are more precise since their uncertainties are always less than those from the RFD. Additionally, both simulations and experimental data confirm that the sum of the coefficients is compatible with one, within measurement errors. This means that second order terms are negligible, thus validating the theoretical linear model outlined in section 3.

Concerning the BATJ coefficients for VB WP, it is worth noticing that c_1 and c_2 are negative and, consequently, c_3 is larger than one. Observing VB3 and VB6 we notice an increase for c_1 and c_2 and a decrease for c_3. This comes from the fact that we are moving the phase towards the crest.

Table 4: BATJ coefficients for VB WP.

	VB		
	RFD	EOS	Sim
c_1	-0.09 ± 0.12	-0.16 ± 0.05	-0.12
c_2	-0.12 ± 0.11	-0.04 ± 0.08	-0.05
c_3	1.15 ± 0.11	1.15 ± 0.08	1.08
c_4			0.00
$\sum_{i=1}^{4} c_i$	0.94 ± 0.33	0.95 ± 0.21	0.91

Table 5: BATJ coefficients for VB3 and VB6 WPs.

	VB3			VB6		
	RFD	EOS	Sim	RFD	EOS	Sim
c_1	0.03 ± 0.10	0.04 ± 0.06	0.06	0.05 ± 0.10	0.12 ± 0.05	0.13
c_2	0.01 ± 0.08	0.04 ± 0.05	0.04	-0.04 ± 0.09	0.02 ± 0.04	0.02
c_3	1.04 ± 0.12	1.01 ± 0.08	0.96	0.84 ± 0.11	0.87 ± 0.08	0.80
c_4			0.00			0.00
$\sum_{i=1}^{4} c_i$	1.07 ± 0.30	1.09 ± 0.19	1.06	0.85 ± 0.29	1.02 ± 0.17	0.95

5.2. Interpretation of the results

Once validated with simulations and experimental measurements, the simple linear model for the BATJ is useful to understand which is the most critical sub-system, from a BATJ point of view, for a given WP. In this way, if the beam stability performance at the interaction point must be increased for a certain experiment, then a mitigation strategy could be planned on the source impacting the most.

The obtained BATJ coefficients are used to validate the proposed model with BATJ measurements. Considering the source jitters reported in table 1, table 6 compares measured and estimated jitters. For the estimations, the simulated BATJ coefficients in table 4 are considered and, according to the instrument used for the measurement, i.e., RFD or EOS, model (8) or (9) is applied. Overall, the estimated BATJ results reported in table 6 well reply the measured BATJ, thus confirming the effectiveness of the proposed model.

Table 6: BATJ measurements (Meas.) and estimations (Est.).

WP	RFD jitter [fs]		EOS jitter [fs]	
	Meas.	Est. (8)	Meas.	Est. (9)
VB	113	103	97	100
VB3	91	92	80	88
VB6	77	81	72	75

6. Conclusions

In this paper, the beam jitter model in a linear photo-injector is validated by means of a dedicated experimental run at the SPARC_LAB facility at INFN-LNF laboratories. Beam dynamics simulations validate both the measurements and the theoretical model.

The BATJ coefficients for three WPs have been measured and computed, finding an excellent agreement between experiments and simulations. Once validated, the proposed linear model is used to reproduce the BATJ obtained by the accelerator diagnostics devices, considering the phase jitters of the facility sub-systems. In this way, the model allows to estimate the main sources of noise that have a stronger impact on the stability of an experiment, i.e., on a specific WP. This tool also helps to implement an effective jitter mitigation strategy intervening only on the sources impacting the most.

Furthermore, an extensive benchmarking dedicated to the simulation code was conducted for the specific case of computing BATJ coefficients. The benchmarking could be potentially extended to other simulation codes to compare accuracy, a current hot topic in accelerator physics. Eventually, present work could be extended to model the on crest WP, where amplitude jitter is also expected to play a role.

References

[1] Gschwendtner E and Muggli P 2019 *Nature Reviews Physics* **1** 246–248
[2] Seddon E, Clarke J, Dunning D, Masciovecchio C, Milne C, Parmigiani F, Rugg D, Spence J, Thompson N, Ueda K *et al.* 2017 *Reports on Progress in Physics* **80** 115901
[3] Pompili R, Anania M, Bellaveglia M, Biagioni A, Castorina G, Chiadroni E, Cianchi A, Croia M, Di Giovenale D, Ferrario M *et al.* 2016 *New Journal of Physics* **18** 083033
[4] Craievich P, Di Mitri S, Milloch M, Penco G and Rossi F 2013 *Physical Review Special Topics-Accelerators and Beams* **16** 090401
[5] Franssen J and Luiten O 2017 *Structural Dynamics* **4** 044026
[6] Zhao L, Tang H, Lu C, Jiang T, Zhu P, Hu L, Song W, Wang H, Qiu J, Jing C *et al.* 2020 *Physical review letters* **124** 054802
[7] Alberdi Esuain B, Hwang J G, Neumann A and Kamps T 2022 *Scientific Reports* **12** 13365
[8] Young L M 2023 TStep An electron linac design code (ed. LMY TECHNOLOGY)
[9] Ferrario M, Alesini D, Anania M, Bacci A, Bellaveglia M, Bogdanov O, Boni R, Castellano M, Chiadroni E, Cianchi A *et al.* 2013 *Nuclear Instruments and Methods in Physics Research Section B: Beam Interactions with Materials and Atoms* **309** 183–188
[10] Ferrario M, Alesini D, Bacci A, Bellaveglia M, Boni R, Boscolo M, Calvani P, Castellano M,

Chiadroni E, Cianchi A *et al.* 2011 *Nuclear Instruments and Methods in Physics Research Section A: Accelerators, Spectrometers, Detectors and Associated Equipment* **637** S43–S46
[11] Villa F, Cialdi S, Anania M, Gatti G, Giorgianni F and Pompili R 2014 *Nuclear Instruments and Methods in Physics Research Section A: Accelerators, Spectrometers, Detectors and Associated Equipment* **740** 188–192
[12] Cianchi A, Alesini D, Bacci A, Bellaveglia M, Boni R, Boscolo M, Castellano M, Catani L, Chiadroni E, Cialdi S *et al.* 2008 *Physical Review Special Topics-Accelerators and Beams* **11** 032801
[13] Anderson S, Musumeci P, Rosenzweig J, Brown W, England R, Ferrario M, Jacob J, Thompson M, Travish G, Tremaine A *et al.* 2005 *Physical review special topics-accelerators and beams* **8** 014401
[14] Pompili R, Anania M, Bellaveglia M, Biagioni A, Bisesto F, Chiadroni E, Cianchi A, Croia M, Curcio A, Di Giovenale D *et al.* 2016 *Nuclear Instruments and Methods in Physics Research Section A: Accelerators, Spectrometers, Detectors and Associated Equipment* **829** 17–23
[15] Ferrario M, Alesini D, Bacci A, Bellaveglia M, Boni R, Boscolo M, Castellano M, Chiadroni E, Cianchi A, Cultrera L *et al.* 2010 *Physical review letters* **104** 054801
[16] Alesini D, Di Pirro G, Ficcadenti L, Mostacci A, Palumbo L, Rosenzweig J and Vaccarezza C 2006 *Nuclear Instruments and Methods in Physics Research Section A: Accelerators, Spectrometers, Detectors and Associated Equipment* **568** 488–502
[17] Pompili R, Cianchi A, Alesini D, Anania M, Bacci A, Bellaveglia M, Castellano M, Chiadroni E, Di Giovenale D, Di Pirro G *et al.* 2014 *Nuclear Instruments and Methods in Physics Research Section A: Accelerators, Spectrometers, Detectors and Associated Equipment* **740** 216–221
[18] Sabato L, Arpaia P, Gilardi A, Mostacci A, Palumbo L and Variola A 2020 *IEEE Transactions on Instrumentation and Measurement* **70** 1–9
[19] Pompili R, Anania M, Bisesto F, Botton M, Castellano M, Chiadroni E, Cianchi A, Curcio A, Ferrario M, Galletti M *et al.* 2016 *Optics Express* **24** 29512–29520
[20] Curcio A, Anania M, Bisesto F, Botton M, Castellano M, Chiadroni E, Cianchi A, Ferrario M, Galletti M, Giulietti D *et al.* 2018 *Physical Review Applied* **9** 024004

Appendix A. Experimental data

Table A1 lists the RFD calibration coefficients. The experimental data from EOS and RFD for all the WPs are gathered in tables from A2 to A7.

Table A1: RFD calibration coefficients.

WP	$\mathrm{Cal_{fit}} \pm \mathrm{Cal_{err}}$ [ps/mm]
OC	1.265 ± 0.008
VB	0.916 ± 0.008
VB3	0.916 ± 0.009
VB6	0.991 ± 0.008

Table A2: Experimental data from the RFD for the VB WP.

	y centroid [mm], $\mathrm{RFD_{read}} \pm \mathrm{RFD_{err}}$		
Phase [°]	Laser	K1	K2
-1	6.98 ± 0.17	5.91 ± 0.11	8.24 ± 0.11
-0.5	7.10 ± 0.13	6.45 ± 0.12	7.77 ± 0.07
0	7.02 ± 0.11	6.94 ± 0.10	7.01 ± 0.12
0.5	7.16 ± 0.17	7.62 ± 0.17	6.45 ± 0.14
1	7.20 ± 0.11	8.32 ± 0.13	5.87 ± 0.08

Table A3: Experimental data from the RFD for the VB3 WP.

	y centroid [mm], $\mathrm{RFD_{read}} \pm \mathrm{RFD_{err}}$		
Phase [°]	Laser	K1	K2
-1	7.26 ± 0.06	6.16 ± 0.12	8.28 ± 0.12
-0.5	7.30 ± 0.09	6.71 ± 0.08	7.70 ± 0.09
0	7.23 ± 0.07	7.24 ± 0.10	7.17 ± 0.11
0.5	7.19 ± 0.09	7.80 ± 0.11	6.63 ± 0.11
1	7.25 ± 0.14	8.27 ± 0.07	6.06 ± 0.11

Table A4: Experimental data from the RFD for the VB6 WP.

	y centroid [mm], $\mathrm{RFD_{read}} \pm \mathrm{RFD_{err}}$		
Phase [°]	Laser	K1	K2
-1	8.15 ± 0.10	7.17 ± 0.09	9.11 ± 0.05
-0.5	8.20 ± 0.06	7.76 ± 0.10	8.59 ± 0.07
0	8.14 ± 0.06	8.25 ± 0.10	8.24 ± 0.05
0.5	8.10 ± 0.04	8.69 ± 0.08	7.87 ± 0.09
1	8.09 ± 0.10	9.25 ± 0.05	7.44 ± 0.13

Table A5: Experimental data from the EOS for the VB WP.

	time [ps], $\mathrm{EOS_{read}} \pm \mathrm{EOS_{err}}$ (delay line [mm])		
Phase [°]	Laser	K1	K2
-1	4.54 ± 0.09 (81.2)	4.17 ± 0.11 (81.1)	4.44 ± 0.07 (80.9)
-0.5	4.06 ± 0.04 (81.2)	4.28 ± 0.09 (81.1)	4.37 ± 0.06 (81.0)
0	4.52 ± 0.11 (81.0)	4.07 ± 0.10 (81.1)	4.21 ± 0.15 (81.1)
0.5	4.13 ± 0.14 (81.0)	4.22 ± 0.10 (81.1)	4.23 ± 0.11 (81.2)
1	4.36 ± 0.07 (80.9)	4.12 ± 0.16 (81.1)	3.96 ± 0.08 (81.3)

Table A6: Experimental data from the EOS for the VB3 WP.

Phase [°]	time [ps], $EOS_{read} \pm EOS_{err}$ (delay line [mm])		
	Laser	K1	K2
-1	4.01 ± 0.08 (80.8)	3.74 ± 0.07 (80.7)	3.97 ± 0.08 (80.5)
-0.5	4.10 ± 0.07 (80.7)	3.76 ± 0.06 (80.7)	3.92 ± 0.05 (80.6)
0	3.69 ± 0.09 (80.7)	3.80 ± 0.08 (80.7)	4.32 ± 0.06 (80.6)
0.5	3.93 ± 0.07 (80.6)	3.84 ± 0.09 (80.7)	4.17 ± 0.12 (80.7)
1	4.04 ± 0.11 (80.5)	3.82 ± 0.07 (80.7)	3.96 ± 0.10 (80.8)

Table A7: Experimental data from the EOS for the VB6 WP.

Phase [°]	time [ps], $EOS_{read} \pm EOS_{err}$ (delay line [mm])		
	Laser	K1	K2
-1	4.12 ± 0.09 (80.4)	4.01 ± 0.07 (80.3)	3.86 ± 0.06 (80.2)
-0.5	3.84 ± 0.07 (80.4)	3.97 ± 0.07 (80.3)	3.71 ± 0.07 (80.3)
0	3.99 ± 0.05 (80.3)	3.99 ± 0.07 (80.3)	4.00 ± 0.05 (80.3)
0.5	4.16 ± 0.06 (80.2)	4.03 ± 0.05 (80.3)	3.75 ± 0.09 (80.4)
1	3.89 ± 0.08 (80.2)	4.02 ± 0.07 (80.3)	3.62 ± 0.12 (80.5)